UHF RFID Localization Based on Phase Evaluation of Passive Tag Arrays

Martin Scherhäufl, *Graduate Student Member, IEEE*, Markus Pichler, *Member, IEEE*, and Andreas Stelzer, *Member, IEEE*

***Abstract*— This paper presents a 2-D localization system based on phase-of-arrival evaluation of passive ultrahigh frequency (UHF) radio frequency identification (RFID) transponders. To handle the ambiguity caused by phase evaluation, several tags are arranged to form a uniform linear array. A multiple input multiple output system, where sequentially each frontend is configured to work as transmitter, while the remaining frontends serve as receivers, is used to enable position estimation. For proof of concept, a local position measurement system demonstrator was built comprising conventional passive EPCglobal Class-1 Gen-2 UHF RFID tags, one commercial off-the-shelf RFID reader, several transceiver frontends, baseband hardware, and signal processing. Measurements were carried out in an indoor office environment, where the 3.5 m × 2.5 m measurement zone was surrounded by drywalls and concrete floor and ceiling, and the experimental results showed robust and accurate localization with a root-mean-square deviation of 0.011 m and a maximum error of 0.032 m. These experimental results were confirmed by simulations, which were performed to determine the limits of the system accuracy.**

***Index Terms*— Linear antenna arrays, phase estimation, position measurement, radiofrequency identification (RFID), RFID tags, ultrahigh frequency (UHF) technology.**

I. Introduction

MANY modern applications use radio frequency identification (RFID) as a wireless noncontact method of data transfer to identify and track the objects to which the transponders are attached. Since passive tags can be used, which collect the energy from the interrogating electromagnetic field created by RFID readers, the transponders require no local power sources such as batteries. This results in reduced need for maintenance while achieving high flexibility, long lifetime, and low cost.

Manuscript received May 13, 2014; revised August 29, 2014; accepted September 30, 2014. This work was supported in part by the Austrian COMET-K2 programme of the Linz Center of Mechatronics, in part by the Austrian Federal Government, and in part by the Federal State of Upper Austria. The Associate Editor coordinating the review process was Dr. Maciej Zawodniok.

M. Scherhäufl is with the Department of Sensors and Communication, Linz Center of Mechatronics, Linz 4040, Austria (e-mail: martin.scherhaeufl@lcm.at).

M. Pichler is with the Department of Sensors and Communication, Linz Center of Mechatronics, Linz 4040, Austria (e-mail: markus.pichler@lcm.at).

A. Stelzer is with the Institute for Communications Engineering and RF-Systems, Johannes Kepler University Linz, Linz 4040, Austria (e-mail: a.stelzer@nthfs.jku.at).

Color versions of one or more of the figures in this paper are available online at http://ieeexplore.ieee.org.

Digital Object Identifier 10.1109/TIM.2014.2363578

Although in many cases, knowledge about the presence of an object is sufficient, reliable information about the accurate position would lead to enhanced possibilities. In recent years, various systems have been presented, which allow localization of RFID transponders [1]–[4]. The method probably used most often derives the estimate of the tag position from the transmission level or the signal strength received by stationary receivers [5]–[8]. Based on the k-nearest neighbor principle, localization systems for passive ultrahigh frequency (UHF) RFID transponders have been presented in [9] and [10]. These systems evaluate the received signal strength indicator (RSSI) at the RFID reader and compare this value with the RSSI of numerous reference tags at fixed and known locations. A probabilistic model for tracking of RFID transponders at an RFID gate is introduced in [11], where a hidden Markov model (HMM) is used to cover both the stochastic nature of read events and the dynamic of a typical identification process within the gate. The HMM is based on the RSSI, which depends on the relative position and orientation of the tag with respect to the reader antenna. In [12], a mobile robot navigation system is presented, where the direction of arrival of the received signal from a transponder is evaluated using the ratio of the received signal strength between two adjacent antennas. This enables the robot to continuously monitor the changes in transponder directions and ensures reliable docking guidance to the target transponder.

Since cluttering, multipath propagation, tag orientation, and environmental conditions have a strong impact on signal strength, systems using sensor fusion promise increased localization accuracy and robustness. In [13], a system for probabilistic tag localization based on fusion of RFID and computer vision is presented. A similar approach is introduced in [14], where data using vision-based range sensors and RFID technology are combined.

Several approaches to track mobile devices equipped with RFID readers are presented in [15]–[17], where numerous reference transponders are placed at fixed and known locations. The coordinates of the mobile device can be determined by the location of the transponders that communicate with the reader.

A system based on time-of-flight measurements, where the quality of the localization results depends on the signal waveform, is introduced in [18]. If a standardized protocol is used for communication and if the current regulations are met, this principle of measurement is, however, unsuitable for localization in most cases because of the limited signal bandwidth.

Several RFID localization systems rely on phase evaluation of the tag response signal. Compared with the signal strength, the phase of arrival (PoA) is usually less influenced by clutter, multipath propagation, and environmental conditions, which in general, leads to more accurate position estimates. If antenna arrays are used, the transponder can be localized based on the angle of arrival (AoA) of the received signal or by performing beam steering [19]–[23]. Since the unwrapped PoA is proportional to the length of the propagation path, localization of the transponder is enabled by PoA evaluation. As there is a 2π ambiguity in phase measurement, systems using a constant carrier frequency require a large number of different signal paths to achieve robust and accurate position estimation [24]. Other approaches avoid the ambiguity of phase measurement by evaluating the PoA using different carrier frequencies, which leads to absolute distance measurements [25]–[28]. However, the accuracy of these systems depend on the available bandwidth, which is limited by regulatory standards. Several RFID localization systems rely on coherent superposition of phase values sampled by synthetic apertures [29] or inverse synthetic apertures [30], [31], where movement of either the reader antenna or the transponder is required.

In this paper, a 2-D localization system based on phase evaluation of passive UHF RFID transponders is presented. To handle the 2π ambiguity of phase measurement, the RFID tags are arranged to form a uniform linear array (ULA) whose orientation in azimuth is estimated simultaneously with its position. For proof of concept, a local position measurement system demonstrator comprising conventional UHF RFID tags, one commercial off-the-shelf RFID reader, several transceiver frontends, baseband hardware, and signal processing was used for measurements in an indoor office environment. Compared with the currently popular methods, where only a single RFID tag is used for localization, this system offers better accuracy, sensitivity, and robustness while meeting the regulatory standards.

II. System Description

To allow robust and accurate localization, N passive UHF RFID transponders are arranged to form a ULA. If a query round is initiated by an RFID reader using one of the K frontends of the multiple input multiple output (MIMO) system demonstrator, the transponders sequentially communicate information containing their unique identification number by means of backscatter modulation, where the reflection coefficient of the tag antenna is switched between two stages in accordance with the data being sent. The backscattered signals are received by the remaining $K-1$ frontends, amplified by low-noise amplifiers (LNAs), down-converted to baseband, and recorded by analog-to-digital converters (ADCs). This results in M intermediate frequency (IF) signals, one for each combination of transmit and receive antenna. Since these signals contain the unique identification number of the tags, a PoA can be assigned to each of the N transponders and M channels of the measurement system. As each PoA depends on the length of the signal path from the transmit antenna via the RFID tag to the receive antenna, position and orientation of the ULA can be estimated.

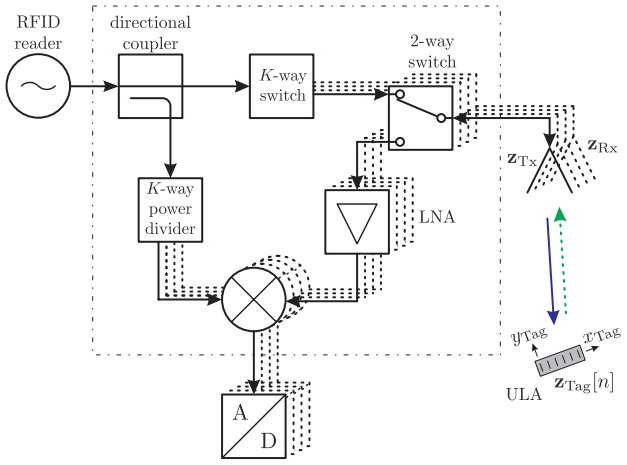

Fig. 1. Schematic representation of the local position measurement system consisting of K frontends.

III. Measurement Apparatus

We designed a MIMO system demonstrator, whose system architecture can be observed in schematic representation in Fig. 1. A commercial off-the-shelf RFID reader configured to use a standardized protocol for identifying the passive UHF RFID transponders generates the transmit signal. This signal feeds to the common port of a K-way switch, which–together with 2-way-switches–selects the frontend used for communication between reader and tag. The backscattered tag signals occurring at the remaining $K-1$ frontends, which are configured as receivers, are amplified by LNAs and support the radio frequency inputs of quadrature demodulators, one on each channel. The local oscillator inputs of these demodulators are provided by a K-way power divider in combination with a directional coupler, which is located in the transmission line. The resulting complex IF signals are acquired simultaneously by a multichannel ADC card.

IV. Signal Model

As presented in [32], the parameters of the IF signal occurring at the mth channel of the measurement system are its amplitude A and PoA φ, and can therefore be considered to form a complex vector $\tilde{s}$

$$\tilde{s}[m] = A[m]e^{j\varphi[m]} \tag{1}$$

where $1 \leq m \leq M$, and M is the number of channels defined by

$$M = K(K-1) \tag{2}$$

with K representing the number of frontends. To avoid confusion, we use a tilde to denote a complex quantity. If N RFID tags are present in the measurement zone, the signal model extends to

$$\tilde{s}[m,n] = A[m,n]e^{j\varphi[m,n]} \tag{3}$$

with $1 \leq n \leq N$. The PoA is described by

$$\varphi[m,n] = \frac{2\pi}{\lambda}(r_{\mathrm{Tx}}[m,n] + r_{\mathrm{Rx}}[m,n]) + \varphi_{\mathrm{off}}[m,n] \tag{4}$$

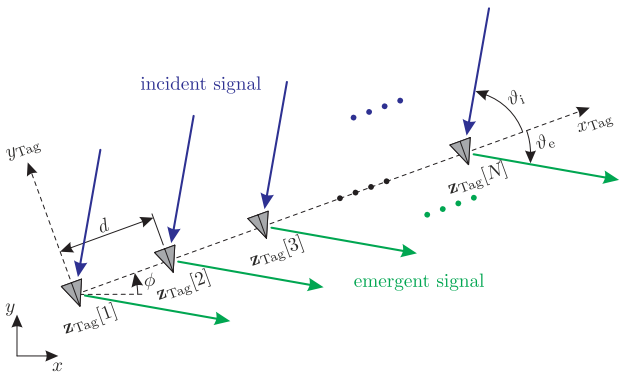

Fig. 2. ULA of N passive UHF RFID tags.

where λ is the wavelength of the transmitted radio frequency signal, and r_{Tx}, r_{Rx} is the Euclidean distance between the corresponding antenna of the frontend and the RFID tag

$$r_{\mathrm{Tx}}[m,n] = \|\mathbf{z}_{\mathrm{Tx}}[m] - \mathbf{z}_{\mathrm{Tag}}[n]\| \tag{5}$$

$$r_{\mathrm{Rx}}[m,n] = \|\mathbf{z}_{\mathrm{Rx}}[m] - \mathbf{z}_{\mathrm{Tag}}[n]\|. \tag{6}$$

Since an additional phase offset φ_{off} occurs that depends on various factors including cable length, characteristics of the system demonstrator, and tag characteristics, calibration is necessary to enable localization by means of PoA evaluation.

A. RFID Tag Array

To allow accurate and robust localization using phase evaluation, the N RFID tags are arranged to form a ULA with element spacing d, as shown in Fig. 2. For each channel of the measurement system, the incident wave causes a spatial frequency ξ_{i} at the tag array, which depends on its position and orientation

$$\xi_{\mathrm{i}}[m] = \frac{1}{\lambda}\cos(\vartheta_{\mathrm{i}}[m]). \tag{7}$$

Due to the reciprocity of the system, the emergent wave can also be considered to be the cause of a spatial frequency ξ_{e}

$$\xi_{\mathrm{e}}[m] = \frac{1}{\lambda}\cos(\vartheta_{\mathrm{e}}[m]). \tag{8}$$

It is implied that the spatial frequencies are constant values for the entire ULA, which is a reasonable assumption if far-field conditions dominate and if the RFID transponders show similar backscatter characteristics. Combined with the element spacing d, the spatial frequencies lead to a normalized frequency ψ occurring at adjacent tags for each channel of the measurement system

$$\begin{aligned}\psi[m] &= d(\xi_{\mathrm{i}}[m] + \xi_{\mathrm{e}}[m]) \\ &= \frac{d}{\lambda}(\cos(\vartheta_{\mathrm{i}}[m]) + \cos(\vartheta_{\mathrm{e}}[m])).\end{aligned} \tag{9}$$

To prevent ψ from changing by more than 1/2, the spacing d must be chosen in accordance with the Nyquist criterion

$$d < \frac{\lambda}{2|\cos(\vartheta_{\mathrm{i}}[m]) + \cos(\vartheta_{\mathrm{e}}[m])|}. \tag{10}$$

Since the orientation ϕ of the ULA is not restricted and the incident and emergent angles ϑ_{i} and ϑ_{e} can therefore vary between 0 and 2π, the element spacing d is limited by

$$d < \frac{\lambda}{4}. \tag{11}$$

The fact that the sampled frequency caused by the backscattered tag signals of adjacent transponders of the ULA is described by ψ is considered in the signal model by

$$\tilde{s}[m,n] \approx \tilde{s}'[m,n] = A[m]e^{j\left(\varphi_0[m] + 2\pi\,\psi[m]\left(n - \frac{N+1}{2}\right)\right)} \tag{12}$$

where φ_0 is the PoA in the center of the ULA. For simplification, the signal amplitude A has been approximated to be equal for all tags. Due to several factors including multipath propagation, cluttering, and environmental conditions, it is assumed that the signal is overlaid with complex white Gaussian noise (CWGN) $\tilde{w}$ with variance σ^2

$$\tilde{w}[m,n] \sim \mathcal{CN}(0,\sigma^2) \tag{13}$$

and this leads to the data set

$$\tilde{x}[m,n] = \tilde{s}'[m,n] + \tilde{w}[m,n]. \tag{14}$$

B. Parameter Estimation of the Tag Array

Since the N RFID tags are arranged to form a ULA, an estimation of the parameters of the IF signals

$$\boldsymbol{\theta}_{\mathrm{IF}}[m] = \begin{bmatrix} A[m] & \varphi_0[m] & \psi[m] \end{bmatrix}^T \tag{15}$$

according to the data model described by (14) is required for each channel of the measurement system. Since for deriving the estimator one channel is sufficient to show the mode of operation, the subscript m is omitted for better readability. Naturally, the estimation must be performed for all channels. For complex signals in CWGN with variance σ^2, the probability density function (pdf) is defined by

$$\begin{aligned} p_{\mathrm{IF}}(\tilde{\mathbf{x}};\boldsymbol{\theta}_{\mathrm{IF}}) &= \prod_{n=1}^{N} \frac{1}{\pi\sigma^2} e^{-\frac{1}{\sigma^2}|\tilde{x}[n] - \tilde{s}'[n;\boldsymbol{\theta}_{\mathrm{IF}}]|^2} \\ &= \frac{1}{\pi^N \det(\sigma^2\mathbf{I})} e^{-\frac{1}{\sigma^2}(\tilde{\mathbf{x}} - \tilde{\mathbf{s}}'(\boldsymbol{\theta}_{\mathrm{IF}}))^H(\tilde{\mathbf{x}} - \tilde{\mathbf{s}}'(\boldsymbol{\theta}_{\mathrm{IF}}))} \end{aligned} \tag{16}$$

where H denotes the conjugate transpose [33]. The maximum likelihood estimation (MLE) is defined by the values of $\boldsymbol{\theta}_{\mathrm{IF}}$ that maximize p_{IF}, which corresponds to the parameters found by minimizing the cost function

$$J_{\mathrm{IF}}(\tilde{\mathbf{x}};\boldsymbol{\theta}_{\mathrm{IF}}) = (\tilde{\mathbf{x}} - \tilde{\mathbf{s}}'(\boldsymbol{\theta}_{\mathrm{IF}}))^H(\tilde{\mathbf{x}} - \tilde{\mathbf{s}}'(\boldsymbol{\theta}_{\mathrm{IF}})). \tag{17}$$

If we define

$$\tilde{a} = Ae^{j\varphi_0} \tag{18}$$

$$\tilde{\mathbf{B}} = \begin{bmatrix} e^{j2\pi\psi\frac{1-N}{2}} & e^{j2\pi\psi\frac{3-N}{2}} & \cdots & e^{j2\pi\psi\frac{N-1}{2}} \end{bmatrix}^T \tag{19}$$

the parameters can be separated and the cost function can be written as

$$J'_{\mathrm{IF}}(\tilde{\mathbf{x}};\tilde{a},\psi) = (\tilde{\mathbf{x}} - \tilde{\mathbf{B}}\tilde{a})^H(\tilde{\mathbf{x}} - \tilde{\mathbf{B}}\tilde{a}). \tag{20}$$

Hence, the result of minimizing the cost function of the linear model over $\tilde{a}$ is

$$\hat{\tilde{a}} = (\tilde{\mathbf{B}}^H\tilde{\mathbf{B}})^{-1}\tilde{\mathbf{B}}^H\tilde{\mathbf{x}} \tag{21}$$

and thus

$$\begin{aligned} J''_{\mathrm{IF}}(\tilde{\mathbf{x}};\hat{\tilde{a}},\psi) &= (\tilde{\mathbf{x}}-\tilde{\mathbf{B}}\hat{\tilde{a}})^H(\tilde{\mathbf{x}}-\tilde{\mathbf{B}}\hat{\tilde{a}}) \\ &= \tilde{\mathbf{x}}^H\tilde{\mathbf{x}} - \tilde{\mathbf{x}}^H\tilde{\mathbf{B}}(\tilde{\mathbf{B}}^H\tilde{\mathbf{B}})^{-1}\tilde{\mathbf{B}}^H\tilde{\mathbf{x}}. \end{aligned} \tag{22}$$

To find $\hat{\psi}$, the function J''_{IF} must be minimized over ψ or, equivalently, the function

$$\tilde{\mathbf{x}}^H\tilde{\mathbf{B}}(\tilde{\mathbf{B}}^H\tilde{\mathbf{B}})^{-1}\tilde{\mathbf{B}}^H\tilde{\mathbf{x}} \tag{23}$$

must be maximized. Using the definition of $\tilde{\mathbf{B}}$, the MLE for ψ is found by

$$\hat{\psi} = \arg\max_{\psi} \frac{1}{N}\left|\sum_{n=1}^{N}\tilde{x}[n]e^{-j2\pi\,\psi\left(n-\frac{N+1}{2}\right)}\right|^2 \tag{24}$$

which can be achieved by applying a fast Fourier transform. Applying this result to (21), the parameter $\hat{\tilde{a}}$ can be calculated by

$$\hat{\tilde{a}} = \frac{1}{N}\sum_{n=1}^{N}\tilde{x}[n]e^{-j2\pi\,\hat{\psi}\left(n-\frac{N+1}{2}\right)} \tag{25}$$

which finally leads to

$$\hat{A} = |\hat{\tilde{a}}| = \frac{1}{N}\left|\sum_{n=1}^{N}\tilde{x}[n]e^{-j2\pi\,\hat{\psi}\left(n-\frac{N+1}{2}\right)}\right| \tag{26}$$

$$\hat{\varphi}_0 = \angle\hat{\tilde{a}} = \arctan\frac{\mathrm{Im}\left(\sum_{n=1}^{N}\tilde{x}[n]e^{-j2\pi\,\hat{\psi}\left(n-\frac{N+1}{2}\right)}\right)}{\mathrm{Re}\left(\sum_{n=1}^{N}\tilde{x}[n]e^{-j2\pi\,\hat{\psi}\left(n-\frac{N+1}{2}\right)}\right)}. \tag{27}$$

V. Position Estimation

Based on the data set $\tilde{\mathbf{x}}$, the position and the orientation of the ULA must be estimated. The parameter vector is specified by

$$\boldsymbol{\theta} = [x \quad y \quad \phi]^T. \tag{28}$$

It is assumed that the PoA is influenced by additional white Gaussian noise (AWGN), and therefore the pdf is defined by

$$p(\tilde{\mathbf{x}};\boldsymbol{\theta}) = \frac{1}{(2\pi)^{\frac{NM}{2}}\det^{\frac{1}{2}}(\mathbf{C}_\varphi)}e^{-\frac{1}{2}(\angle\tilde{\mathbf{x}}-\boldsymbol{\varphi}(\boldsymbol{\theta}))^T\mathbf{C}_\varphi^{-1}(\angle\tilde{\mathbf{x}}-\boldsymbol{\varphi}(\boldsymbol{\theta}))} \tag{29}$$

where $\mathbf{C}_\varphi$ is a diagonal matrix specifying the variances of the phase measurements, which can be approximated by

$$\mathbf{C}_\varphi \approx \sigma^2(\mathrm{diag}|\tilde{\mathbf{x}}|)^{-2} \tag{30}$$

and $\boldsymbol{\varphi}$ is a vector containing the theoretical PoAs of the calibrated system as described by (4). The MLE is defined by the values of $\boldsymbol{\theta}$ that maximize p, which corresponds to the parameters found by minimizing the cost function

$$J(\tilde{\mathbf{x}};\boldsymbol{\theta}) = (\angle\tilde{\mathbf{x}}-\boldsymbol{\varphi}(\boldsymbol{\theta}))^T\mathbf{C}_\varphi^{-1}(\angle\tilde{\mathbf{x}}-\boldsymbol{\varphi}(\boldsymbol{\theta})) \tag{31}$$

where the PoAs must be unwrapped such that the phase difference is within the interval $[-\pi,\pi]$. Hence, the MLE can be expressed by

$$\hat{\boldsymbol{\theta}} = \arg\min_{\boldsymbol{\theta}}(\angle\tilde{\mathbf{x}}-\boldsymbol{\varphi}(\boldsymbol{\theta}))^T\mathbf{C}_\varphi^{-1}(\angle\tilde{\mathbf{x}}-\boldsymbol{\varphi}(\boldsymbol{\theta})). \tag{32}$$

Finding the MLE is therefore a nonlinear problem. Since the existence of an analytic solution is very unlikely and the convergence of iterative algorithms cannot be guaranteed due to phase ambiguity, a numerical grid search approach is used. Finding the MLE requires discretization in all parameters, which results in excessive computational effort. Simplification of the algorithm is therefore desired.

A. Utility Function

Introducing a utility function

$$\begin{aligned} P(\boldsymbol{\theta}) &= \mathrm{Re}\left(\tilde{\mathbf{x}}^H\mathbf{W}e^{j\boldsymbol{\varphi}(\boldsymbol{\theta})}\right) \\ &= \sum_{m=1}^{M}\sum_{n=1}^{N}|\tilde{x}[m,n]|^2\cos(\angle\tilde{x}[m,n]-\varphi[m,n;\boldsymbol{\theta}]) \end{aligned} \tag{33}$$

where $\mathbf{W}$ is a diagonal matrix containing the amplitudes of $\tilde{\mathbf{x}}$, reduces the computational effort significantly, since the calculation basically becomes a matrix multiplication. Furthermore, with this algorithm, it is no longer necessary that the phase difference be within the interval $[-\pi,\pi]$. Using the second-order Taylor series for the cosine function, the utility function can be approximated by

$$\begin{aligned} P(\boldsymbol{\theta}) \approx &\sum_{m=1}^{M}\sum_{n=1}^{N}|\tilde{x}[m,n]|^2 \\ &-\sum_{m=1}^{M}\sum_{n=1}^{N}\frac{|\tilde{x}[m,n]|^2}{2}(\angle\tilde{x}[m,n]-\varphi[m,n;\boldsymbol{\theta}])^2 \end{aligned} \tag{34}$$

where the first term is not influenced by $\boldsymbol{\theta}$ and hence irrelevant for parameter estimation. Using (30), the second term can be written as

$$-\frac{\sigma^2}{2}(\angle\tilde{\mathbf{x}}-\boldsymbol{\varphi}(\boldsymbol{\theta}))^T\mathbf{C}_\varphi^{-1}(\angle\tilde{\mathbf{x}}-\boldsymbol{\varphi}(\boldsymbol{\theta})) \tag{35}$$

and is therefore a negative and scaled version of (31). Hence, an approximation of the MLE is found, where the parameters $\boldsymbol{\theta}$ are estimated by

$$\hat{\boldsymbol{\theta}} = \arg\max_{\boldsymbol{\theta}}\mathrm{Re}(\tilde{\mathbf{x}}^H\mathbf{W}e^{j\boldsymbol{\varphi}(\boldsymbol{\theta})}). \tag{36}$$

B. Estimation of the Orientation of the ULA

The ϕ-dimension of the grid search algorithm can be reduced if the orientation is calculated based on the estimates for the spatially sampled frequency $\boldsymbol{\psi}$ for each position of the grid. If we define

$$\boldsymbol{\alpha} = [\Delta x \quad \Delta y]^T \tag{37}$$

$$\mathbf{H} = \frac{1}{2\pi}\left[\frac{\partial\boldsymbol{\varphi}(\boldsymbol{\theta})}{\partial x} \quad \frac{\partial\boldsymbol{\varphi}(\boldsymbol{\theta})}{\partial y}\right] \tag{38}$$

the signal model for the spatially sampled frequency $\boldsymbol{\psi}$ caused by adjacent RFID tags of the ULA is

$$\boldsymbol{\psi} = \mathbf{H}\boldsymbol{\alpha}. \tag{39}$$

If the signal model is assumed to be overlaid with AWGN, where $\mathbf{C}_\psi$ is the covariance matrix belonging to the estimates of $\hat{\boldsymbol{\psi}}$ according to (24), the pdf is

$$p_\phi(\hat{\boldsymbol{\psi}};\boldsymbol{\alpha}) = \frac{1}{(2\pi)^{\frac{M}{2}}\det^{\frac{1}{2}}(\mathbf{C}_\psi)} e^{-\frac{1}{2}(\hat{\boldsymbol{\psi}}-\mathbf{H}\boldsymbol{\alpha})^T\mathbf{C}_\psi^{-1}(\hat{\boldsymbol{\psi}}-\mathbf{H}\boldsymbol{\alpha})}. \tag{40}$$

The MLE is defined as the values of $\boldsymbol{\alpha}$ that maximize the pdf, which is equivalent to the parameters found by minimizing the cost function

$$J_\phi(\hat{\boldsymbol{\psi}};\boldsymbol{\alpha}) = (\hat{\boldsymbol{\psi}} - \mathbf{H}\boldsymbol{\alpha})^T\mathbf{C}_\psi^{-1}(\hat{\boldsymbol{\psi}} - \mathbf{H}\boldsymbol{\alpha}). \tag{41}$$

Hence, minimization of the cost function over $\boldsymbol{\alpha}$ of the linear model leads to the solution

$$\hat{\boldsymbol{\alpha}} = [\hat{\Delta x}\ \ \hat{\Delta y}]^T = \left(\mathbf{H}^T\mathbf{C}_\psi^{-1}\mathbf{H}\right)^{-1}\mathbf{H}^T\mathbf{C}_\psi^{-1}\hat{\boldsymbol{\psi}}. \tag{42}$$

Based on these estimates, the MLE for the orientation ϕ of the ULA for the corresponding position can be calculated by

$$\hat{\phi} = \arctan\frac{\hat{\Delta y}}{\hat{\Delta x}}. \tag{43}$$

C. Application of the Simplifications

Computational effort can be reduced considerably, if the grid search algorithm is applied to the signal model specified by (12). Based on the estimates of the PoA in the center of the ULA $\hat{\boldsymbol{\varphi}}_0$, the utility function depends on the position $\boldsymbol{\beta} = [x\ \ y]^T$ of the ULA and can be expressed similarly to (33) by

$$P'(\boldsymbol{\beta}) = \mathrm{Re}\left((e^{j\hat{\boldsymbol{\varphi}}_0})^H\mathbf{C}_{\varphi_0}^{-1}e^{j\boldsymbol{\varphi}_0(\boldsymbol{\theta})}\right) \tag{44}$$

and is therefore independent of the orientation ϕ of the ULA. The vector $\boldsymbol{\varphi}_0$ describes the theoretical PoAs of the calibrated system in the center of the ULA calculated by (4), and $\mathbf{C}_{\varphi_0}$ is a diagonal matrix containing the variances belonging to the $\hat{\boldsymbol{\varphi}}_0$ estimates. Hence, the position of the ULA can be estimated using

$$\hat{\boldsymbol{\beta}} = \arg\max_{\boldsymbol{\beta}} \mathrm{Re}\left((e^{j\hat{\boldsymbol{\varphi}}_0})^H\mathbf{C}_{\varphi_0}^{-1}e^{j\boldsymbol{\varphi}_0(\boldsymbol{\theta})}\right). \tag{45}$$

Applying this estimator reduces the ϕ-dimension of the grid search algorithm and thus also the computational effort. However, the robustness of the position estimates decreases significantly. This is shown in Fig. 3, which illustrates the utility function of the estimator. As can be observed, there are several high peaks, of which the highlighted one shows the highest value for P' but belongs to an incorrect position estimate. Nevertheless, the results are adequate for calculating a set of potential positions. Note that this algorithm can be used as an approximation of the MLE for the localization of a single RFID tag if the utility function is evaluated [32].

Applying the MLE of the orientation of the ULA to these potential positions using (42) results in an enhanced utility function that considers the entire information contained in the data set

$$P''(\hat{\boldsymbol{\theta}}) = \mathrm{Re}\left(\tilde{\mathbf{x}}^H\hat{\tilde{\mathbf{s}}}'(\boldsymbol{\theta})\right). \tag{46}$$

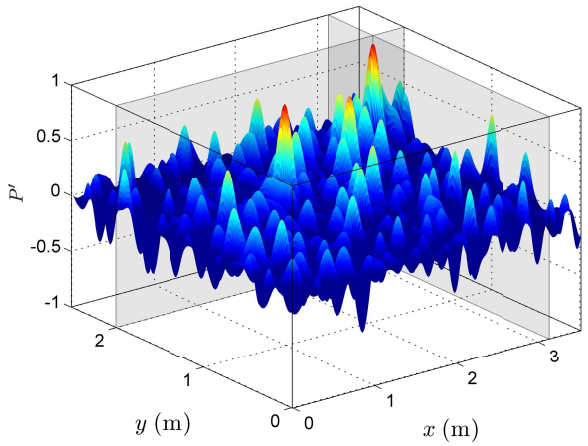

Fig. 3. Utility function P' used for localization based on the PoA estimates $\hat{\boldsymbol{\varphi}}_0$ in the center of the ULA, which consists of $N = 6$ RFID tags. The measurements were carried out in an indoor office environment and are based on $K = 8$ frontends.

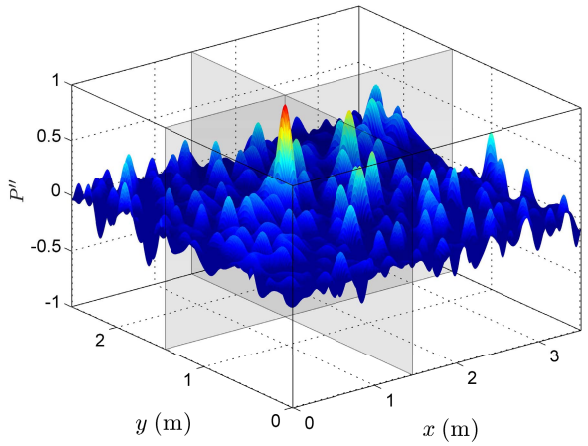

Fig. 4. Utility function P'' used for localization based on PoA evaluation of the ULA, which consists of $N = 6$ RFID tags. The measurements were carried out in an indoor office environment and are based on $K = 8$ frontends.

The signal model $\hat{\tilde{s}}'$ using the estimates of $\boldsymbol{\theta}_{\mathrm{IF}}$ of the ULA is specified by

$$\hat{\tilde{s}}'[m,n;\boldsymbol{\theta}] = \hat{A}[m]e^{j\left(\varphi_0[m;\boldsymbol{\theta}]+2\pi\,\hat{\psi}'[m;\boldsymbol{\theta}]\left(n-\frac{N+1}{2}\right)\right)} \tag{47}$$

and $\hat{\boldsymbol{\psi}}'$ is the MLE for the spatially sampled frequency of the corresponding position, which depends on the estimated $\hat{\boldsymbol{\alpha}}$

$$\begin{aligned}\hat{\boldsymbol{\psi}}' &= \mathbf{H}\hat{\boldsymbol{\alpha}} \\ &= \mathbf{H}\left(\mathbf{H}^T\mathbf{C}_\psi^{-1}\mathbf{H}\right)^{-1}\mathbf{H}^T\mathbf{C}_\psi^{-1}\hat{\boldsymbol{\psi}}.\end{aligned} \tag{48}$$

Hence, the parameters $\boldsymbol{\theta}$ of the ULA can be estimated as the values that maximize the utility function

$$\hat{\boldsymbol{\theta}} = \arg\max_{\boldsymbol{\theta}} \mathrm{Re}\left(\tilde{\mathbf{x}}^H\hat{\tilde{\mathbf{s}}}'(\boldsymbol{\theta})\right). \tag{49}$$

This leads to a significant improvement in robustness compared with the estimator specified in (45). The utility function of the position estimation is shown in Fig. 4, where for illustration purposes, all positions were considered to be estimates of potential positions $\boldsymbol{\beta}$ of the ULA. In contrast to Fig. 3, correct position estimation is achieved.

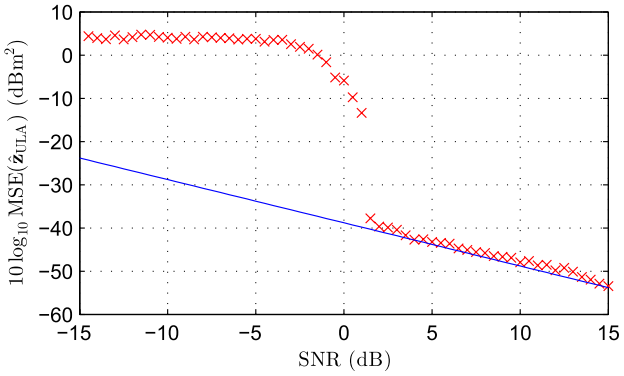

Fig. 5. Simulation of the accuracy of the estimator using the Monte Carlo method. ——: CRLB. ×: simulated MSE of the position estimates.

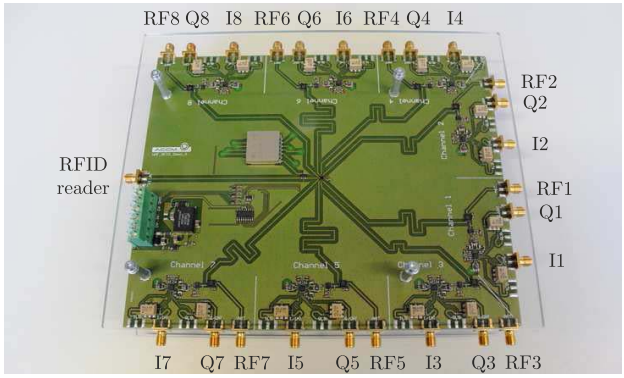

Fig. 6. System demonstrator designed to support $K = 8$ frontends. RF# is the antenna port, and I# and Q# are the outputs of the demodulator for in-phase and quadrature, respectively.

VI. Simulation Results

Simulations using the Monte Carlo method were carried out to evaluate the performance of the estimator specified by (49). A 2-D localization system using a measurement zone defined by 3.5 m × 2.5 m, $K = 8$ frontends, and a ULA consisting of $N = 6$ RFID transponders was simulated, where the distance between adjacent tags was set to $d = 0.06$ m. The data set was overlaid with CWGN, as described by (14). Since the main disturbance occurring at a specific channel is due to multipath propagation, which is assumed to be constant during a measurement cycle, the CWGN was considered to be correlated for individual measurements. The Cramér–Rao lower bound (CRLB), which states the minimum variance that can be achieved by an unbiased estimator, was used as a benchmark to which the performance of the estimator was compared. As shown in Fig. 5, the mean squared error (MSE) of the position estimates depends on the signal-to-noise ratio (SNR). Starting with an SNR threshold level of approximately 1.5 dB, the estimator asymptotically achieves the CRLB.

VII. Experimental Results

A. Experimental Setup

To evaluate the performance of the localization system, measurements were carried out in an indoor office environment that was surrounded by drywalls and a concrete floor and ceiling. To this end, a system demonstrator consisting of $K = 8$ frontends was built, leading to $M = 56$ channels of the measurement system. The system demonstrator is shown in Fig. 6.

The corresponding linearly polarized antennas were distributed at a height of 1.7 m above the floor around the 2-D measurement zone that was defined as 3.5 m × 2.5 m. An EPCglobal Class-1 Gen-2/ISO 1800-6C compliant UHF RFID reader was used to communicate with a ULA of $N = 6$ linearly polarized passive UHF RFID transponders, where the distance between adjacent tags was chosen to be $d = 0.06$ m. The ULA, which was attached to a 2-D traversing rail by means of a plastic frame, was moved to $I = 645$ defined positions in the transceive antenna plane.

The RFID reader was configured to generate a transmit signal using a carrier frequency of 866.9 MHz and a signal level of 2 W equivalent radiated power. The measurement setup is shown in Fig. 7. A strong line-of-sight propagation is present in this scenario. However, several static reflections and multipath propagation generated by drywalls, concrete floor, and ceiling are expected.

Fig. 7. Measurement setup of the localization system consisting of $K = 8$ frontends and a ULA of $N = 6$ UHF RFID tags.

As previously mentioned, calibration is necessary to enable localization by means of phase evaluation. To this end, reference measurements using known transponder positions were carried out, whereas a comparison of the measured values with the calculated values of the PoA leads to estimates for the phase offset $\boldsymbol{\varphi}_{\mathrm{off}}$ according to (4).

B. Localization Results

Applying the simplified algorithm as described in (45), where only one phase value is used for position estimation, the ULA can be localized with less computational effort based on the $\hat{\boldsymbol{\varphi}}_0$ estimates. The root-mean-square deviation (RMSD) of the localization results of the center of the ULA

$$\mathrm{RMSD}(\hat{\mathbf{z}}_{\mathrm{ULA}}) = \sqrt{\frac{\sum_{i=1}^{I} \|\mathbf{z}_{\mathrm{ULA},i} - \hat{\mathbf{z}}_{\mathrm{ULA},i}\|^2}{I}} \tag{50}$$

evaluated to 0.36 m. The localization results can be observed in Fig. 8. As previously mentioned, this algorithm can also be used to localize a single RFID transponder, which leads to similar results [32].

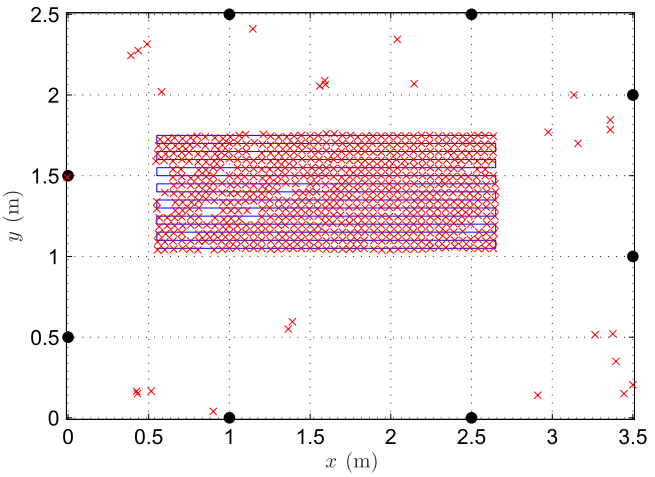

Fig. 8. Simplified localization of the ULA by means of evaluating one phase value per channel. •: antenna position. —: actual track of the ULA. ×: estimated transponder position.

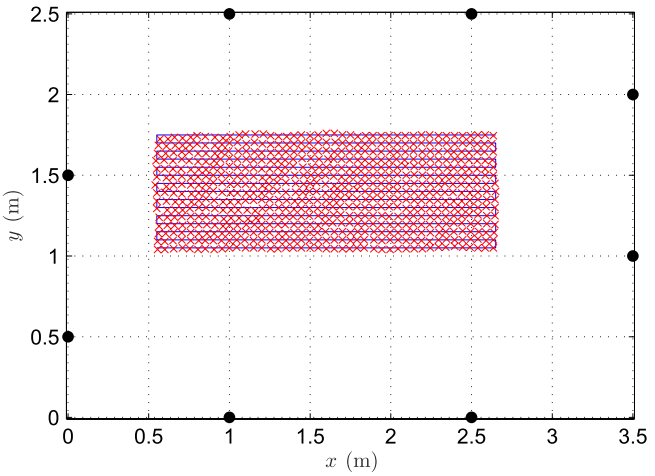

Fig. 9. Accurate Localization of the ULA by means of phase evaluation in an indoor environment. •: antenna position. —: actual track of the ULA. ×: estimated transponder position.

As described above, these results are used only as part of the estimator specified by (49). By applying this algorithm, both the position and orientation of the ULA can be estimated at the cost of slightly increased computational effort. As can be observed in Fig. 9, the robustness of the position estimation is significantly improved. The RMSD of the localization results using this estimator was 0.011 m and the maximum error 0.032 m. Figs. 10 and 11 plot the distribution of the localization error in the x- and y-directions, respectively. As can be observed, the localization error shows similar characteristics for both directions. The distribution of the Euclidean distance of the localization error is shown in Fig. 12.

Since the applied algorithm also estimates the orientation ϕ of the ULA, we calculated their RMSD and the maximum absolute error, which were 0.064 and 0.34 rad, respectively. The distribution of the error of the estimates for ϕ is shown in Fig. 13.

Note that the measurements showed an SNR of approximately 5.3 dB, which is significantly higher than the threshold

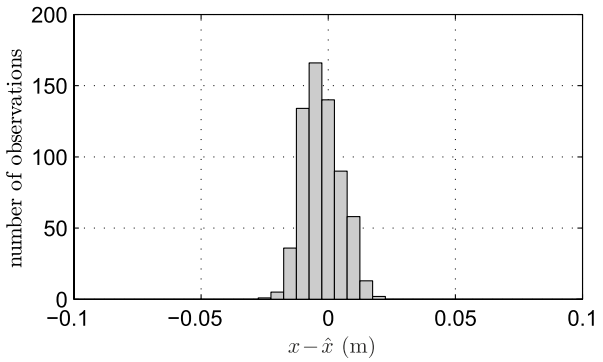

Fig. 10. Distribution of the localization error in the x-direction based on $I = 645$ measurements using a ULA of $N = 6$ RFID tags.

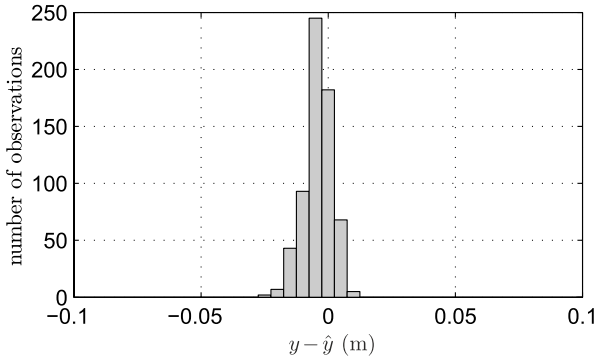

Fig. 11. Distribution of the localization error in the y-direction based on $I = 645$ measurement using a ULA of $N = 6$ RFID tags.

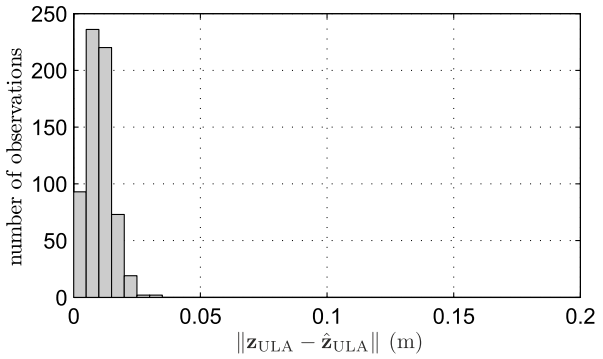

Fig. 12. Distribution of the localization error based on $I = 645$ measurements using a ULA of $N = 6$ RFID tags.

level of 1.5 dB determined by simulations. Therefore, even in scenarios with a more dominant multipath, localization of the ULA would remain feasible. The minimum variance that can be achieved by the unbiased estimator is given by the CRLB. Using the SNR value determined, the CRLB would lead to a standard deviation of the unbiased position estimator of 0.006 m. However, the measurement results showed an RMSD of 0.011 m. The reason for the difference between these values include that some tag/front-end combinations did not produce a tag response, and therefore localization accuracy is reduced.

As previously mentioned, the computational effort of methods using a numerical grid search algorithm can be substantial.

TABLE I
COMPARISON OF LOCALIZATION METHODS

Reference	Target	Approach	Average Accuracy	Measurement Zone	Note
Errington *et al.* [15]	Reader	RSSI	20.5 cm	N/A	Reference transponders at known positions required; localization accuracy depends on density of RFID tags
Nazari *et al.* [16]	Reader	RSSI	6.5 cm	N/A	Reference transponders at known positions required; localization accuracy depends on density of RFID tags
Gueaieb *et al.* [20]	Reader	AoA	3.4 cm	N/A	RFID tags define a trajectory that is tracked by a mobile robot
Choi *et al.* [9]	Tag	RSSI	20.9 cm	$\leq$ 3 m (1D)	Reference transponders at known positions required; localization of the RFID tags based on the k-nearest neighbor principle
Zhang *et al.* [10]	Tag	RSSI	18 cm	4.2 m x 2.8 m	Reference transponders at known positions required; localization of the RFID tags based on the k-nearest neighbor principle
Azzouzi *et al.* [22]	Tag	AoA	10.7 cm	3 m x 3 m	5 antenna arrays, each consisting of 3 patches, placed at the edge of the measurement zone
Povalac *et al.* [27]	Tag	FD-PDoA	14 cm	$\leq$ 2.5 m (1D)	Evaluation of the PDoA in frequency domain (FD-PDoA); localization accuracy is limited by system bandwidth; system calibration is required
Miesen *et al.* [29]	Tag	Synthetic Apertures	2 cm (lateral); 90 cm (distance)	N/A	Synthetic aperture created by moving reader antenna at known trajectory; PoA evaluation of backscattered transponder signals
Scherhäufl *et al.* [30]	Tag	Inverse Synthetic Apertures	6.4 cm	3.5 m x 2.5 m	Inverse synthetic aperture created by moving transponder; MIMO system consisting of 8 frontends; PoA evaluation of backscattered transponder signals; system calibration is required
Parr *et al.* [31]	Tag	Inverse Synthetic Apertures	1 cm (lateral); 5 cm (distance)	N/A	Inverse synthetic aperture created by moving transponder on conveyor belt with known speed; PoA evaluation of backscattered transponder signals
Scherhäufl *et al.* [32]	Tag	PoA	56 cm (single shot); 3.8 cm (tracking)	3.5 m x 2.5 m	MIMO system consisting of 8 frontends; PoA evaluation of backscattered transponder signals; system calibration is required
System proposed in this paper	Tag	PoA	1.1 cm	3.5 m x 2.5 m	MIMO system consisting of 8 frontends; ULA consisting of 6 RFID tags; PoA evaluation of backscattered transponder signals; system calibration is required

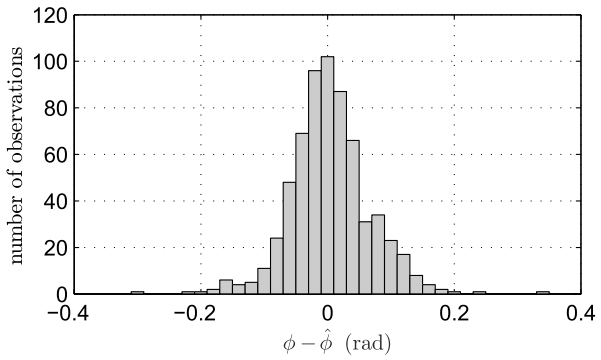

Fig. 13. Distribution of the error of the estimated orientation ϕ based on $I = 645$ measurements using a ULA of $N = 6$ RFID tags.

However, using a grid density of 1 cm and the simplifications described in this paper, the time required for calculating the position and orientation estimates of the ULA can be neglected compared to the time the system takes to sequentially configure each frontend as transmitter and perform a query round by means of the RFID reader.

C. Comparison of Localization Methods

Different RFID localization schemes that provide experimental results are compared in Table I. In summary, no system shows optimum localization characteristics for all cases, and each has its own shortcomings. The analyzed systems using RSSI evaluation offer suitable accuracy, but require numerous reference transponders at fixed and known locations to enable position estimation.

In contrast to these systems, the proposed methods based on phase evaluation do not depend on reference transponders. However, in several cases, a movement of either the reader antenna or the RFID transponder is required to allow accurate and robust position estimation. An exception to this is presented in [22], where the localization is performed by AoA evaluation based on multiple antenna arrays that are placed at the edge of the 2-D measurement zone. This system offers robust position estimation on the cost of user-defined antenna arrays. Another approach, where the distance between reader antenna and RFID tag is estimated based on PDoA evaluation in frequency domain, is introduced in [27]. However, the accuracy of this system depends

on the available bandwidth, which is limited by regulatory standards.

The system presented in this paper offers the highest accuracy of all investigated methods. Furthermore, neither a movement of the reader antennas nor of the RFID transponders is required to allow the position estimation. Compared with the method described in [32], where only a single RFID transponder is used for localization, the robustness of the position estimation is considerably improved. However, since the proposed localization scheme is based on multiple transceiver frontends and a ULA of passive UHF RFID tags, the increased effort required for system installation and calibration has to be mentioned.

VIII. Conclusion

We have presented a 2-D position measurement system for passive UHF RFID tags based on PoA evaluation of the backscattered transponder signals. To handle the 2π ambiguity of phase measurement, the RFID tags are arranged to form a ULA whose position is estimated simultaneously with its position. The system, which combines multiple frontends, uses a commercial off-the-shelf RFID reader and conventional passive EPCglobal Class-1 Gen-2 UHF RFID transponders. Measurements performed by means of a system demonstrator in an indoor office environment surrounded by drywalls and concrete floor and ceiling showed excellent accuracy and robustness for both the position and the orientation of the ULA.

References

[1] P. V. Nikitin, R. Martinez, S. Ramamurthy, H. Leland, G. Spiess, and K. V. S. Rao, "Phase based spatial identification of UHF RFID tags," in *Proc. IEEE Int. Conf. RFID (RFID)*, Apr. 2010, pp. 102–109.

[2] C. Hekimian-Williams, B. Grant, X. Liu, Z. Zhang, and P. Kumar, "Accurate localization of RFID tags using phase difference," in *Proc. IEEE Int. Conf. RFID (RFID)*, Apr. 2010, pp. 89–96.

[3] T. Sanpechuda and L. Kovavisaruch, "A review of RFID localization: Applications and techniques," in *Proc. 5th Int. Conf. Elect. Eng./Electron., Comput., Telecommun. Inf. Technol. (ECTI-CON)*, vol. 2. May 2008, pp. 769–772.

[4] M. Bouet and A. L. dos Santos, "RFID tags: Positioning principles and localization techniques," in *Proc. 1st IFIP Wireless Days*, Nov. 2008, pp. 1–5.

[5] A. R. J. Ruiz, F. S. Granja, J. C. Prieto Honorato, and J. I. G. Rosas, "Accurate pedestrian indoor navigation by tightly coupling foot-mounted IMU and RFID measurements," *IEEE Trans. Instrum. Meas.*, vol. 61, no. 1, pp. 178–189, Jan. 2012.

[6] A. Dionisi, E. Sardini, and M. Serpelloni, "Wearable object detection system for the blind," in *Proc. IEEE Int. Instrum. Meas. Technol. Conf. (I2MTC)*, May 2012, pp. 1255–1258.

[7] A. Athalye, V. Savic, M. Bolic, and P. M. Djuric, "Novel semi-passive RFID system for indoor localization," *IEEE Sensors J.*, vol. 13, no. 2, pp. 528–537, Feb. 2013.

[8] B. Jachimczyk, D. Dziak, and W. J. Kulesza, "RFID—Hybrid scene analysis-neural network system for 3D indoor positioning optimal system arrangement approach," in *Proc. IEEE Int. Instrum. Meas. Technol. Conf. (I2MTC)*, May 2014, pp. 191–196.

[9] J. S. Choi, H. Lee, R. Elmasri, and D. W. Engels, "Localization systems using passive UHF RFID," in *Proc. 5th Int. Joint Conf. INC, IMS IDC (NCM)*, Aug. 2009, pp. 1727–1732.

[10] Z. Zhang, Z. Lu, V. Saakian, X. Qin, Q. Chen, and L.-R. Zheng, "Item-level indoor localization with passive UHF RFID based on tag interaction analysis," *IEEE Trans. Ind. Electron.*, vol. 61, no. 4, pp. 2122–2135, Apr. 2014.

[11] M. Goller and M. Brandner, "Improving classification performance of RFID gates using hidden Markov models," in *Proc. IEEE Instrum. Meas. Technol. Conf. (I2MTC)*, May 2011, pp. 1–5.

[12] M. Kim and N. Y. Chong, "Direction sensing RFID reader for mobile robot navigation," *IEEE Trans. Autom. Sci. Eng.*, vol. 6, no. 1, pp. 44–54, Jan. 2009.

[13] M. Goller, C. Feichtenhofer, and A. Pinz, "Fusing RFID and computer vision for probabilistic tag localization," in *Proc. IEEE Int. Conf. RFID (RFID)*, Apr. 2014, pp. 89–96.

[14] C. Cerrada, S. Salamanca, A. Adan, E. Perez, J. A. Cerrada, and I. Abad, "Improved method for object recognition in complex scenes by fusioning 3-D information and RFID technology," *IEEE Trans. Instrum. Meas.*, vol. 58, no. 10, pp. 3473–3480, Oct. 2009.

[15] A. F. C. Errington, B. L. F. Daku, and A. F. Prugger, "Initial position estimation using RFID tags: A least-squares approach," *IEEE Trans. Instrum. Meas.*, vol. 59, no. 11, pp. 2863–2869, Nov. 2010.

[16] A. A. Nazari Shirehjini, A. Yassine, and S. Shirmohammadi, "An RFID-based position and orientation measurement system for mobile objects in intelligent environments," *IEEE Trans. Instrum. Meas.*, vol. 61, no. 6, pp. 1664–1675, Jun. 2012.

[17] J. H. Cho and M.-W. Cho, "Effective position tracking using B-spline surface equation based on wireless sensor networks and passive UHF-RFID," *IEEE Trans. Instrum. Meas.*, vol. 62, no. 9, pp. 2456–2464, Sep. 2013.

[18] M. S. Trotter and G. D. Durgin, "Range estimation for passive RFID systems that use power-optimized waveforms," in *Proc. IEEE Int. Conf. RFID (RFID)*, Apr. 2012, pp. 102–109.

[19] Y. Zhang, M. G. Amin, and S. Kaushik, "Localization and tracking of passive RFID tags based on direction estimation," *Int. J. Antennas Propag.*, vol. 2007, Oct. 2007, Art. ID 17426.

[20] W. Gueaieb and M. S. Miah, "An intelligent mobile robot navigation technique using RFID technology," *IEEE Trans. Instrum. Meas.*, vol. 57, no. 9, pp. 1908–1917, Sep. 2008.

[21] J. Zhou, H. Zhang, and L. Mo, "Two-dimension localization of passive RFID tags using AOA estimation," in *Proc. IEEE Instrum. Meas. Technol. Conf. (I2MTC)*, May 2011, pp. 1–5.

[22] S. Azzouzi, M. Cremer, U. Dettmar, T. Knie, and R. Kronberger, "Improved AoA based localization of UHF RFID tags using spatial diversity," in *Proc. IEEE Int. Conf. RFID-Technol. Appl. (RFID-TA)*, Sep. 2011, pp. 174–180.

[23] N. Guzey, H. Xu, and S. Jagannathan, "Localization of near-field radio controlled unintended emitting sources in the presence of multipath fading," *IEEE Trans. Instrum. Meas.*, vol. 63, no. 11, pp. 2696–2703, Nov. 2014.

[24] M. Scherhäufl, M. Pichler, D. Müller, A. Ziroff, and A. Stelzer, "Phase-of-arrival-based localization of passive UHF RFID tags," in *Proc. IEEE MTT-S Int. Microw. Symp. Dig. (IMS)*, Jun. 2013, pp. 1–3.

[25] X. Li, Y. Zhang, and M. G. Amin, "Multifrequency-based range estimation of RFID tags," in *Proc. IEEE Int. Conf. RFID (RFID)*, Apr. 2009, pp. 147–154.

[26] D. Arnitz, K. Witrisal, and U. Muehlmann, "Multifrequency continuous-wave radar approach to ranging in passive UHF RFID," *IEEE Trans. Microw. Theory Techn.*, vol. 57, no. 5, pp. 1398–1405, May 2009.

[27] A. Povalac and J. Sebesta, "Phase difference of arrival distance estimation for RFID tags in frequency domain," in *Proc. IEEE Int. Conf. RFID-Technol. Appl. (RFID-TA)*, Sep. 2011, pp. 188–193.

[28] C. Zhou and J. D. Griffin, "Accurate phase-based ranging measurements for backscatter RFID tags," *IEEE Antennas Wireless Propag. Lett.*, vol. 11, pp. 152–155, 2012.

[29] R. Miesen, F. Kirsch, and M. Vossiek, "UHF RFID localization based on synthetic apertures," *IEEE Trans. Autom. Sci. Eng.*, vol. 10, no. 3, pp. 807–815, Jul. 2013.

[30] M. Scherhäufl, M. Pichler, and A. Stelzer, "Localization of passive UHF RFID tags based on inverse synthetic apertures," in *Proc. IEEE Int. Conf. RFID (RFID)*, Apr. 2014, pp. 82–88.

[31] A. Parr, R. Miesen, and M. Vossiek, "Inverse SAR approach for localization of moving RFID tags," in *Proc. IEEE Int. Conf. RFID (RFID)*, Apr. 2013, pp. 104–109.

[32] M. Scherhäufl, M. Pichler, E. Schimbäck, D. Müller, A. Ziroff, and A. Stelzer, "Indoor localization of passive UHF RFID tags based on phase-of-arrival evaluation," *IEEE Trans. Microw. Theory Techn.*, vol. 61, no. 12, pp. 4724–4729, Dec. 2013.

[33] S. Kay, *Fundamentals of Statistical Signal Processing: Estimation Theory*, vol. 1. New York, NY, USA: Prentice-Hall, 1993, ch. 15, pp. 493–554.

Martin Scherhäufl (S'12–GM'14) was born in Linz, Austria, in 1981. He received the Dipl.-Ing. degree in sensors and microsystems from the University of Applied Sciences Upper Austria, Wels, Austria, in 2007. He is currently pursuing the Ph.D. degree with the Institute for Communications Engineering and RF-Systems, Johannes Kepler University of Linz, Linz.

He was with the Department of Industry Automation, Siemens AG, Linz, from 2007 to 2009. Since 2009, he has been with the Department of Sensors and Communication, Linz Center of Mechatronics. His current research interests include system design, signal generation, digital signal processing, and RFID systems.

Markus Pichler (M'09) was born in Linz, Austria, in 1976. He received the Dipl.-Ing. degree in mechatronics and the Dr.Techn. degree from the Johannes Kepler University of Linz, Linz, in 2002 and 2007, respectively.

He was with the Institute for Communications and Information Engineering, University of Linz, Linz, and joined the Linz Center of Mechatronics in 2002. He has authored or co-authored over 40 publications. His current research interests include systems design, signal generation, digital signal processing, and parameter estimation for radar and positioning systems.

Dr. Pichler was the recipient of the 2004 European Microwave Association Radar Prize.

Andreas Stelzer (M'00) was born in Haslach an der Mühl, Austria, in 1968. He received the Dipl.-Ing. degree in electrical engineering from the Technical University of Vienna, Vienna, Austria, in 1994, and the Dr. Techn. (Hons.) (Ph.D.) degree in mechatronics from the Johannes Kepler University of Linz, Linz, Austria, in 2000.

He became an Associate Professor with the Institute for Communications Engineering and RF- Systems, Johannes Kepler University of Linz, in 2003. Since 2008, he has been a Key Researcher with the Austrian Center of Competence in Mechatronics, Linz, where he is responsible for numerous industrial projects. Since 2007, he has been the Head of the Christian Doppler Research Laboratory for Integrated Radar Sensors, and has been a Full Professor with the Johannes Kepler University since 2011, where he heads the Department of RF-Systems. He has authored or co-authored over 320 journal and conference papers. His research is focused on microwave sensor systems for industrial and automotive applications, radar concepts, SiGe-based circuit design currently up to 320 GHz, microwave packaging in eWLB, RF and microwave subsystems, surface acoustic wave sensor systems and applications, and digital signal processing for sensor signal evaluation.

Dr. Stelzer is a member of the Austrian Electrotechnical Association, the IEEE Microwave Theory and Techniques (MTT) Society, the IEEE Instrumentation and Measurement Society, and the IEEE Circuits and Systems Society. He was a recipient of several awards, including the 2008 IEEE MTT Society Outstanding Young Engineer Award, the 2011 IEEE Microwave Prize, the 2012 European Conference on Antennas and Propagation Best Measurement Paper Prize, the 2012 Asia Pacific Conference on Antennas and Propagation Best Paper Award, the 2011 German Microwave Conference Best Paper Award, the EEEfCOM Innovation Award, and the 2003 European Microwave Association Radar Prize of the European Radar Conference. He has served as an Associate Editor of the IEEE MICROWAVE AND WIRELESS COMPONENTS LETTERS. He currently serves as the Co-Chair for MTT-27 Wireless-Enabled Automotive and Vehicular Applications. He will serve as a as the IEEE Distinguished Microwave Lecturer from 2014 to 2016.